Egypt. J. Rad. Sci. Applic. **Vol. 35,** No. 1-2, pp. 57-68 (2022)

Egyptian Journal of Radiation Sciences and Applications
http://ejrsa.journals.ekb.eg/

EGYPTIAN ATOMIC ENERGY AUTHORITY

Electrical Characterization of Irradiated-La0.6Sr0.4Co0.2Fe0.8O3 Cathodes for Intermediate-Temperature SOFCs Applications

Amr Ahmed[(1)#], E. Borham[(1)], M.M. Ibrahim[(1)], Amir A. Mahdy[(2)], Taha Mattar[(3)], I.A. Ali[(4)]

[(1)]Department of Solids, NCRRT, Atomic Energy Authority, Cairo, Egypt; [(2)]Department of Petroleum & Mining, Faculty of Engineering, Al-Azhar University, Cairo, Egypt; [(3)]Department of Steel, Central Metallurgical Research and Development Institute, Cairo, Egypt; [(4)]Department of Nuclear Physics, Cyclotron Facility, Nuclear Research Center, Atomic Energy Authority, Cairo, Egypt.

IDEVELOPING low-polarization and stable cathodes is a key element to the success of intermediate-temperature solid oxide fuel cells (IT-SOFCs). Here we report a study on the electrochemical performance and stability of a $La_{0.6}Sr_{0.4}Co_{0.2}Fe_{0.8}O_{3-\delta}$ (LSCF) cathode material using gamma irradiation approach; with different doses namely, 20kGy, 250kGy and 500 kGy. This is an innovative method; which has an tremendous effect on the Morphology and electrical properties. LSCF cathode samples were systematically characterized using X-ray diffraction (XRD), photoluminescence (PL), high resolution transmission electron microscope (HRTEM), and BET surface area analyzer. The occupancy of oxygen vacancies in the samples was conceded by PL studies. Electrical properties were investigated for both the un irradiated and irradiated (LSCF) samples at various operating temperatures from room temperature up to 400°C.This novel study shows that the cathode performance was strongly influenced by particle size, surface area and formation of oxygen vacancies. All physical and electrical properties for LSCF samples were improved by using gamma radiation approach; which has a high impact on the cell performance.

Keywords: Cathodes, Conductivity, LSCF, Oxygen vacancy, Perovskite, Radiation, Solid oxide fuel cells.

Introduction

Solid oxide fuel cell (SOFC) is an electrochemical device that efficiently converts chemical energy to electrical energy (Mahmud et al., 2017). Commercially available SOFC operates at considerably high temperature (800–1000°C) for stationary applications. The reduction of operating temperature is a breakthrough for SOFC applications in mobile (electronics and transport sector) and portable (military sector) devices (Hussain et al., 2016). Cathode electrode should have large specific surface area for small cathode reaction resistance. That is, cathode electrode should be porous with fine crystal grains. LSCF is one of the most promising cathode materials because it has a high ionic and electronic conductivity, and fast oxygen surface exchange (Katsuki et al., 2003; Wang et al., 2003). $La_{0.6}Sr_{0.4}Co_{0.2}Fe_{0.8}O_{3-\delta}$ (LSCF) is a very interesting material that can work as a cathode for solid-oxide fuel cells and batteries (Laruelle et al., 2000). It is widely used as a cathode material for SOFC in an intermediate temperature range (500–800°C) because of its excellent thermal-chemical stability in contact with ceria-based electrolytes and high electrocatalytic activity in reducing environment (Marinha et al., 2011). LSCF cathode materials can be prepared through several methods, such as solid-state reaction (Richardson et al., 2004), spray pyrolysis (Luyten et al., 2000), sol-gel process (SG) (Hsu & Hwang, 2006), glycine-nitrate process (GNP) (Ghouse et al., 2010), ethylene diamine tetraacetic acid-citrate process

#Corresponding author e-mail: amrhammad0114@gmail.com
Received 10/11/2022; Accepted 19/01/2023
DOI: 10.21608/EJRSA.2023.173853.1141

(Leng et al., 2008), and co-precipitation process (Zhou et al., 2008). Among them, SG is becoming an increasingly popular route for the preparation of SOFC materials (Alber & Cox, 1997; Lev & Wu, 1997). While this approach gives time and energy saving advantages, the main benefit is the formation of highly porous structures, providing very high surface areas, useful for many applications. The SG method also allows the preparation of a mixture in solution, achieving homogeneity on the molecular scale in the solid product. Furthermore, the composition of the oxide can easily be tailored by varying the ratios of the precursors in solution. In general, SG processing allows the control of the texture, composition, homogeneity, and structural properties of the resulting materials, which in turn, influences the structural and electrochemical properties of materials (Liu & Wang, 1995; Wanqin Jin et al., 2000).

Tremendous efforts have been made to alter LSCF cathode microstructure using carbon based dispersing agent into LSCF mixtures in a sol-gel process that is believed to alter the cathode microstructure which will facilitates the electrochemical reaction rates. However, the dispersion activity of carbon-based material is low and surface modification is needed to prevent the agglomeration of cathode powder (Adler, 1998). Morever, to enhance the performance and/or stability of LSCF cathode, several approaches have been studied, including using composite cathode of LSCF-SDC (Hwang et al., 2005; Suzuki et al., 2004) and LSCF-GDC (Murray et al., 2002). Producing the ultrafine cathode powders with a good crystallization, uniform shape, and narrow size distribution is desirable for high cathode performance as it will provide larger active areas for the cathode reactions and consequently reduces the cathode polarization resistance. The polarization resistance of the LSCF cathode significantly depends on the composition, sintering temperature, microstructure, testing environment (fuel and operating temperature), and fabrication methods of the cathode components (Nie et al., 2010).

In the present study; we dispense with these traditional techniques using γ-irradiation. This innovative approach induced synthesis of nanomaterials attracted significant attention due to the following advantages: low energy consumption; minimal use of potentially harmful chemicals; relatively simple synthesis schemes (Berejka, 1995). γ-irradiation has a great effect on morphology and electrochemical properties of LSCF samples which related by formation of oxygen vacancies. Oxygen vacancies in ABO3 perovskite oxides have a direct impact on their crystal structure, electronic property, and surface chemistry. Understanding the role of oxygen vacancies in the oxygen reduction reaction (ORR) is extremely important in terms of design and synthesis of new perovskite oxide catalysts for energy storage and conversion (Qianqian et al., 2020). Oxygen ionic conductivity is ascribed to the concentration of oxygen carrier (oxygen vacancy). The oxide ion conductivity can be improved by the creation of more oxygen vacancies (Cohen, 1992; Jin et al., 1994). The presence of these oxygen vacancies can lead to perovskite oxides exhibiting different physical and chemical properties, including electrocatalytic and photocatalytic properties (Mefford et al., 2014; Bi et al., 2017; Wang et al., 2019). These vacancies also bring a series of catalytic performance improvements to perovskites. LSCF cathode materials should possess adequate oxygen vacancies enabling for the oxygen reduction reaction (ORR) to occur on the whole surface of the cathode not just at the cathode/electrolyte interface or triple phase boundary (TPB). In addition, LSCF perovskite-type membranes have been shown to display 2 to 4 orders of magnitude higher oxygen permeation fluxes than LSM cathodes at identical operating temperatures (Tai et al., 1995). The ionizing effect of gamma radiation may alter the structurally dependent properties of materials and hence their performance. The magnitude of such changes is largely dependent on radiation parameters such as linear energy transfer, dose and energy, nature of the material and its structural phase (Raj Mani et al., 2015).

In this study, the morphological change of $La_{0.6}Sr_{0.4}Co_{0.2}Fe_{0.8}O_{3-\delta}$ (LSCF) electrode was performed using γ- radiation. Specific features focused on are the influences of porosity, particle size, specific surface area and oxygen vacancies on the electrical performance of LSCF cathode.

Experimental

Preparation of LSCF powders:

LSFC powders were synthesized by a Sol-gel and modified sol-gel by irradiation technique. The calculated amounts of $La(NO3)_3$.6H2O (99

%), Sr(NO3)2.6H2O (99 %), $Co(NO3)_2 \cdot 6H2O$ (98.9%) , $Fe(NO3)_3 \cdot 9H2O$ (99%) and urea (98%) as chelating agent, (all from Fluka company) were first dissolved and mixed in a 100 mL of distilled water by magnetic stirring at room temperature. The resultant solution was heated and stirred at 200 °C for 5 h that results in formation of dark brown gel. After that; the yield product was radiated from the sol gel route by different doses of gamma irradiation (20, 250 and 500 kGy), with Cobalt 60 source (Ge 4000A). The Co-60 γ -rays source of NCCRT (India Gamma chamber 4000 A,) was used for the irradiation of the samples. The samples were subjected to γ -rays at room temperature with a dose rate of 1.347 kGy/h. All samples were calcined at 1100°C for 6 h to obtain LSCF powders.

Structural and morphological characterization:

The phase structure of the unirradiated and irradiated LSCF powders was characterized by BET surface area Micromeritics-2020, X-ray diffraction (Philips XPERT) analysis with Cu-Kα (λ=0.1544 nm) radiation with an angle range of 10°≤2θ≤90° and 0.025° step size at room temperature. Photoluminescence spectrometer was employed to analyze the optical characteristics of LSCFsamples at room temperature using a spectrofluorometer (JASCOFR-6500) with an excitation wave length set at λ=240 nm.

Electrical performance analysis

For electrical conductivity measurement, the LSCF powders were pressed into pellet (diameter= 12 mm and thickness=4mm) using uniaxial pressure (50 MPa). The pellet was sintered at 850°C for 2 h in air.The electrical properties of the pellet were measured using a standard two-probe method. Silver paste was applied on the pellet.

The electrical properties of LSCF samples were measured in air from room temperature up to 400 °C. All data were acquired using an LCR meter with the frequency range of 20 Hz up to 5 MHz and wave amplitude of 10 mV.

Results and Discussion

XRD results of LSCF prepared powder:

The X-ray diffraction patterns of the as prepared and LSCF powders after being calcined at 1100°C are shown in Fig. 1. The calcined powders have well crystalline perovskite phase of LSCF and the diffraction peaks can be indexed to (110), (020), (202), (220), (132), (224), (332). All the diffraction peaks can be assigned to single-phase of LSCF with orthorhombic structure (JCPSD 48-0125) (Deshmukh & Bari, 2015). The obtained peaks are in a good agreement with each other .The average crystallite size of the sample was also evaluated from mathematical expression given by Scherrer.

The equation given as:

$$D = K \lambda / \beta \cos \theta$$

where D is the volume mean diameter, K is a constant (=0.94), ß is the integral width, λ is the wavelength (=1.54055 Å), and θ is the diffraction angle (Deshmukh & Bari, 2015). The average crystallite size calculated for the unirradiated and irradiated(20 kGy, 250 kGy and 500 kGy) samples were 19, 18, 27 and 42 respectively.

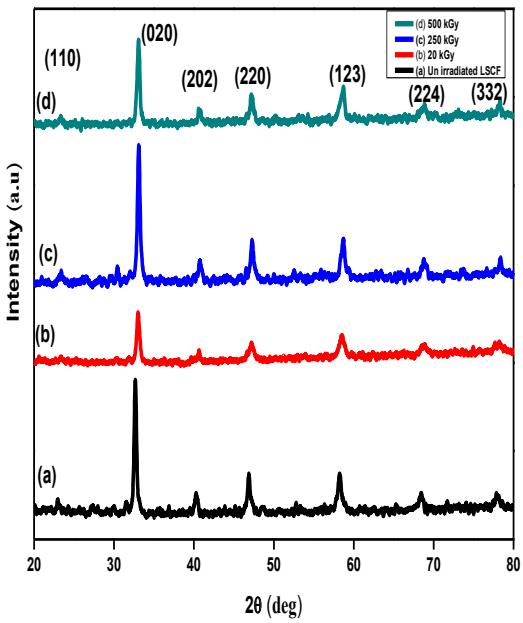

Fig. 1. XRD spectra of (a) unirradiated and irradiated (b), 20kGy (c) 250 kGy, (d) 500 kGy LSCF samples after calcined at 1100°C

BET studies

The specific surface areas were measured using BET analysis to obtain information about the granularity of the synthesized powder.It was observed that 20 KGy irradiated sample has higher surface area, pore size and porosity as mentioned in our published article (Ahmed et al., 2022) compared to other studies (Abd Al-Rahman, 2013).

Field emission electron microscopy:

FESEM was used for examination microstructure for all LSC samples as shown in Fig. 2. It was observed that the un-irradiated sample has a bulky structure while irradiated samples (20 KGy, 250 KGy and 500 KGy) have more refined structure (Ali et al., 2012).

DRS spectra

Diffuse reflectance of the un irradiated and irradiated LSCF samples studied in ultraviolet–visible range (200–800 nm) and NIR range (760-2500 nm) by using JASCO-V570 spectrophotometer. Kubelka Munk function is converted the diffuse reflectance spectroscopy data of powder into equivalent absorption coefficients (α) (Zhu et al., 2016). Kubelka Munk function (K-M) is given by the following equation:

$$F(R) = (K\text{-}M)=\alpha=(1\text{-}R)^2/2R$$

where R is the reflectance data of all LSCF samples, F(R) is Kubelka Munk function, α is absorption coefficients. The band gap of the prepared powder can be determined (Ng et al., 2010; Anand et al., 2013) using the following equation:

$$(F(R)h\upsilon) = (\alpha h\upsilon) = A(h\upsilon\text{-}Eg)^Z$$

where h is constant, F(R) is Kubelka Munk function, F(hυ) is energy function, R is the reflectance of the samples, α is absorption coefficients, Eg is band gap energy and Z is the value between 1/2, 3/2, 2 and 3 depending on the direct allowed, direct forbidden, indirect allowed and indirect forbidden electronic transitions, respectively (Tandon & Gupta, 1970). The diffuse reflectance spectra for the irradiated LSCF sample (i.e. 20 kGy) is shown as an representative example in Fig. 3.The indirect band gap energy (Eg) of the 20 kGy irradiated sample has been determined by plotting $[F(R)* h\nu]^{0.5}$ *vs* hν and extrapolating the linear part of the curve $[F(R)* h\nu]^{0.5}$ to zero as shown in Fig. 4. The calculated indirect band gap of the unirradiated and irradiated LSCF samples ranged between 2.27-2.48 ev are shown in Table 1. From Eg values, it is clear that the band gap of 2.27 eV for the un irradiated LSCF has widened with radiation to about 2.48 eV for irradiated LSCF samples except for 500 kGy sample; which may be attributed to the increase in crystallites size than other irradiated samples as was discussed in a published article (Ahmed et al., 2022). This optical band gap widening can be attributed to existence of large numbers of defects and or oxygen vacancies. We concluded that band gap energy increased by radiation due to increasing the concentration of oxygen vacancies; which contrary to the concept that oxygen vacancies would reduce the apparent band gap (Sreeram et al., 2008). Similar results of blue shift band gaps due to oxygen vacancies have been previously reported in literature (Kaur et al., 2018). By comparison, the calculated values of the activation energy in a published review (Ahmed et al., 2022) and optical band gaps energy for investigated LSCF samples could be noticed that values of an electrical activation energy were very small compared with the optical band gap energy which indicate that oxygen vacancies acts as electron donors in our samples and marked n-type semi conductor.

Photoluminescence spectroscopy

PL spectroscopy is an effective method to identify the existence of different types of defects and vacancies in qLSCF powder. The Photoluminescence characteristics were determined at room temperature using a spectrofluorometer (JASCO FP-6500) with an excitation wave length set at λ=240 nm ; which was higher than the optical gap of our samples. (Ismariza et al., 2020) demonstrated that the 480 and 600 nm emission peaks originate from defect electronic states formed by surface oxygen vacancies and 435 nm luminescence emission peaks from the in-plan oxygen vacancies. AS shown in Fig. 5, all LSCF samples have a strong green photoluminescence (PL) at room temperature; where the emission peak located at 480 nm is related to the combination of holes with two electron trape oxygen vacancies (V_O). Morever, the PL intensity for irradiated samples was decreased than irradiated one due to radiation; which led to formation of high oxygen vacancies (Adler et al., 2007; Kernazhitsky et al., 2017; Abd Malek et al., 2020).

Electrochemical analysis:

Electrochemical impedance spectroscopy (EIS) was employed to evaluate the area-specific polarization resistance (ASR) of LSCF samples as a function of temperature in air; the instrument used to perform EIS was LCR meter. The frequency was swept from 5 MHz to 20 Hz under a zero DC bias with an AC perturbation amplitude of 1V. The temperature dependence of RP was studied from room temperature to 400°C.

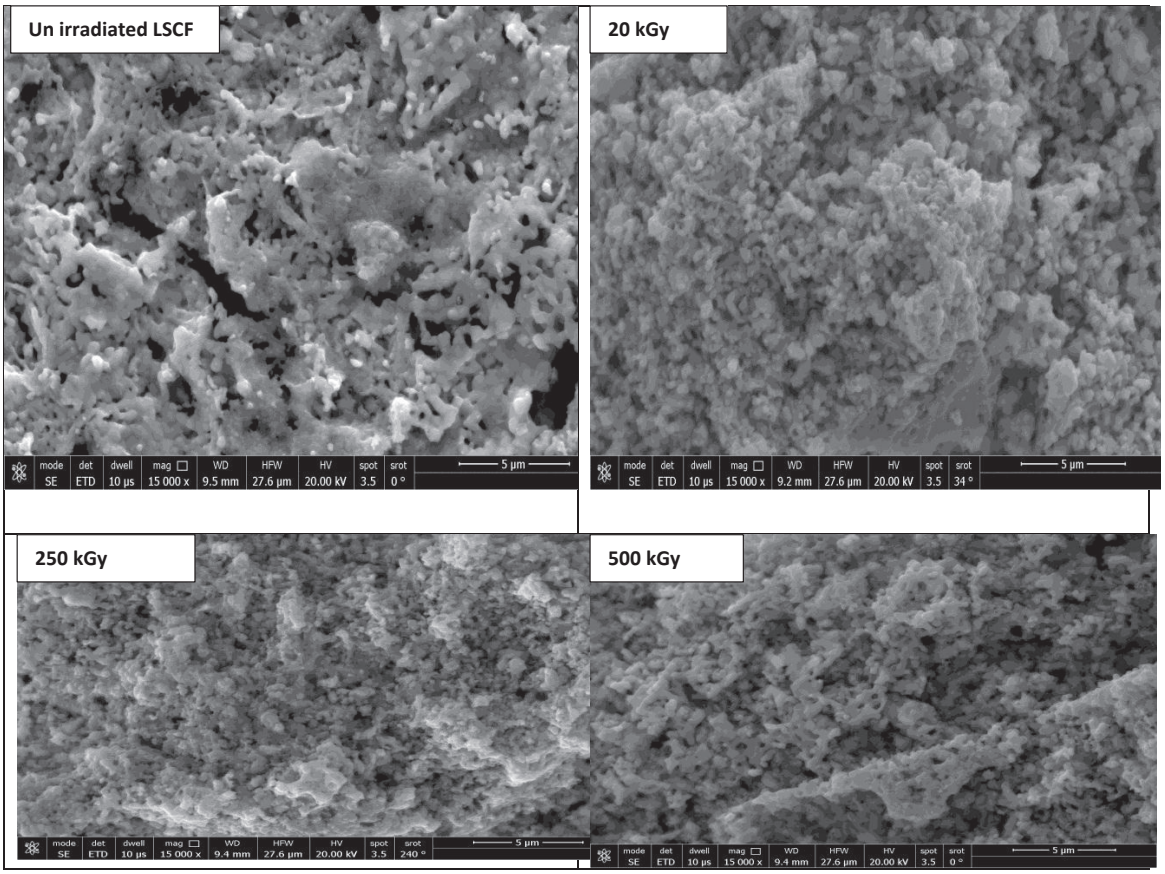

Fig. 2. FESEM for un irradiated and Irradiated LSCF samples calcined at 1100°C

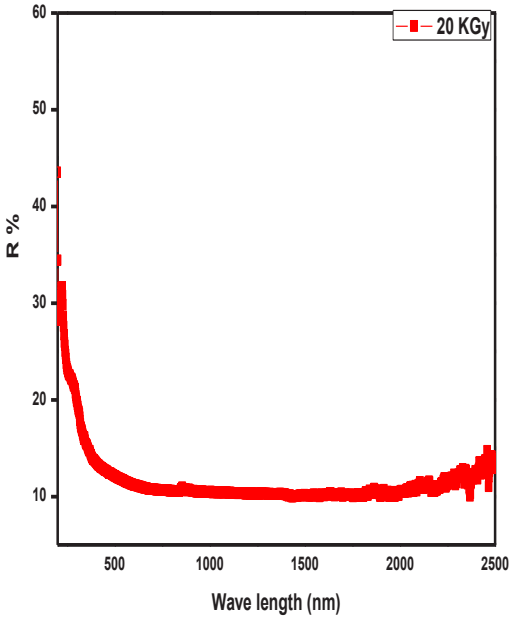

Fig. 3. Diffuse reflectance spectra of irradiated LSCF sample

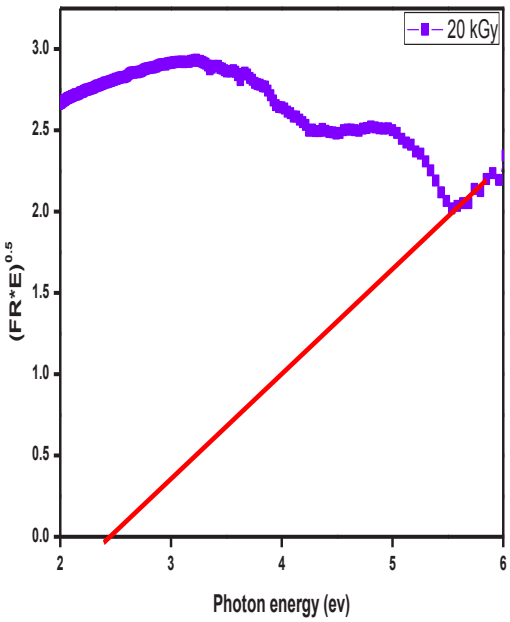

Fig. 4. Band gap of 20 kGy sample calcined at 1100°C

TABLE 1. Band gap energy and calculated activation energy for all LSCF samples

LSCF Sample	Band gap energy (Eg); ev from DRS	Activation Energy (Ea), ev
Un irradiated	2.27	$2.045 *10^{-4}$
20 kGy	2.42	$2.013*10^{-4}$
250 kGy	2.48	$1.698*10^{-4}$
500 kGy	2.43	$1.8836*10^{-4}$

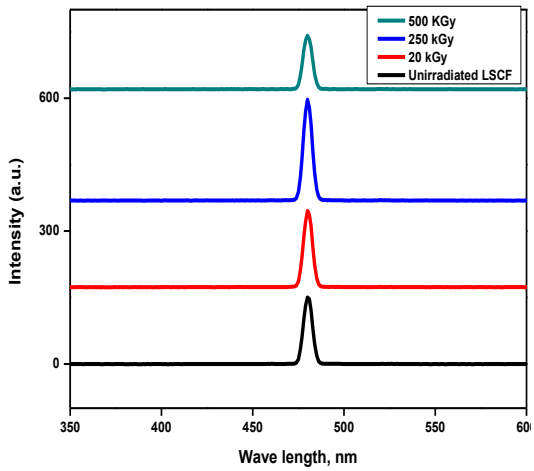

Fig. 5. PL spectra for un-irradiated and irradiated LSCF sample

Nyquist plot

The EIS data were further analyzed by fitting the Nyquist plots with Z-plot software using the equivalent circuit shown in Fig. 6 (a, b, c and d) at different temperatures, from which RP (the length on the Z′-axis intersected by the arc) is determined. This nyquist plot represents a parallel equivalent circuit; which consist of resistor and capacitor for all LSCF samples at different temperatures. As expected, all the impedances decrease with the increase of temperature. The resultant arc in nyquist plot was indicated to ORR; according to pervious studies (Perry Murray et al., 2002; Gu et al., 2009; Ali et al., 2012). These arcs in all LSCF samples were led to information about oxygen diffusion and dissociation processes determinate the ORR rate (Ismariza et al., 2020). The polarization resistance (Rp) at high frequency arc is related to charge (ion and electron) transfer resistances occurring at the current collector/cathode interfaces.

Polarization resistance

Polarization resistance (Rp) was decreased with raising temperature and decreased frequency for all LSCF as shown in Fig. 7. This was considered very important parameter that determined the cathode performance in terms of the interfacial polarization resistance, and generally reported in terms of the area specific resistance (ASR). The polarization resistance (Rp) was determined by the EIS analysis. The ASR of the electrode reactions is calculated using the relation ASR = RP × S/2, where S is defined as the effective surface area of the electrode and the factor 1/2 takes into account that symmetrical sample were used. The ASR values determined for the LSCF cathode samples are presented in Table 2. From these results; it can be deduced that the highest performance cathode material which evidenced by the lowest ASR value exhibited at 4000C (i.e. 20 KGy); which is also of higher surface area and oxygen vacancy formation.The lowest ASR is associated with extension of TPB. This result is excellently compared by other studies (Abd Malek et al., 2020; Ismariza et al., 2020).

Electrical conductivity

The electrical conductivity of the LSCF sintered pellets as a function of operating temperature (°C) was investigated as shown in Fig. 8. In general, the total electrical conductivity of the MIEC is the sum of electronic and ionic conductivity, which are closely associated with electron hole and oxygen vacancies (Kostogloudis & Ftikos, 1999). However, the ionic conductivity, in this type of oxides, is lower than the electronic conductivity. Therefore, it can be assumed reasonably that the measured values refer to the electronic conductivity alone (Yin et al., 2014). The formation of electron holes and oxygen vacancies in the LSCF is due to increase in the substitution of divalent cations, such as Sr^{2+} for La^{3+} (El-Mallah,, 2012). So in LSCF, the electronic compensation is induced by raising the valence of B-site cations forms electronic holes (e,g., Fe^{4+} and Co^{4+} cations), and ionic compensation forms oxygen vacancies (Kostogloudis & Ftikos, 1999). It was observed from our results that conductivity increases with raising temperatures for all LSCF samples. As shown in Table 3 that 20 kGy has a great maximum electrical conductivity value at high temperatures than other samples. It was also clearly that radiation mechanism had a big role in improving conductivity as porosity, particle size, surface area and formation of the oxygen vacancies increased.

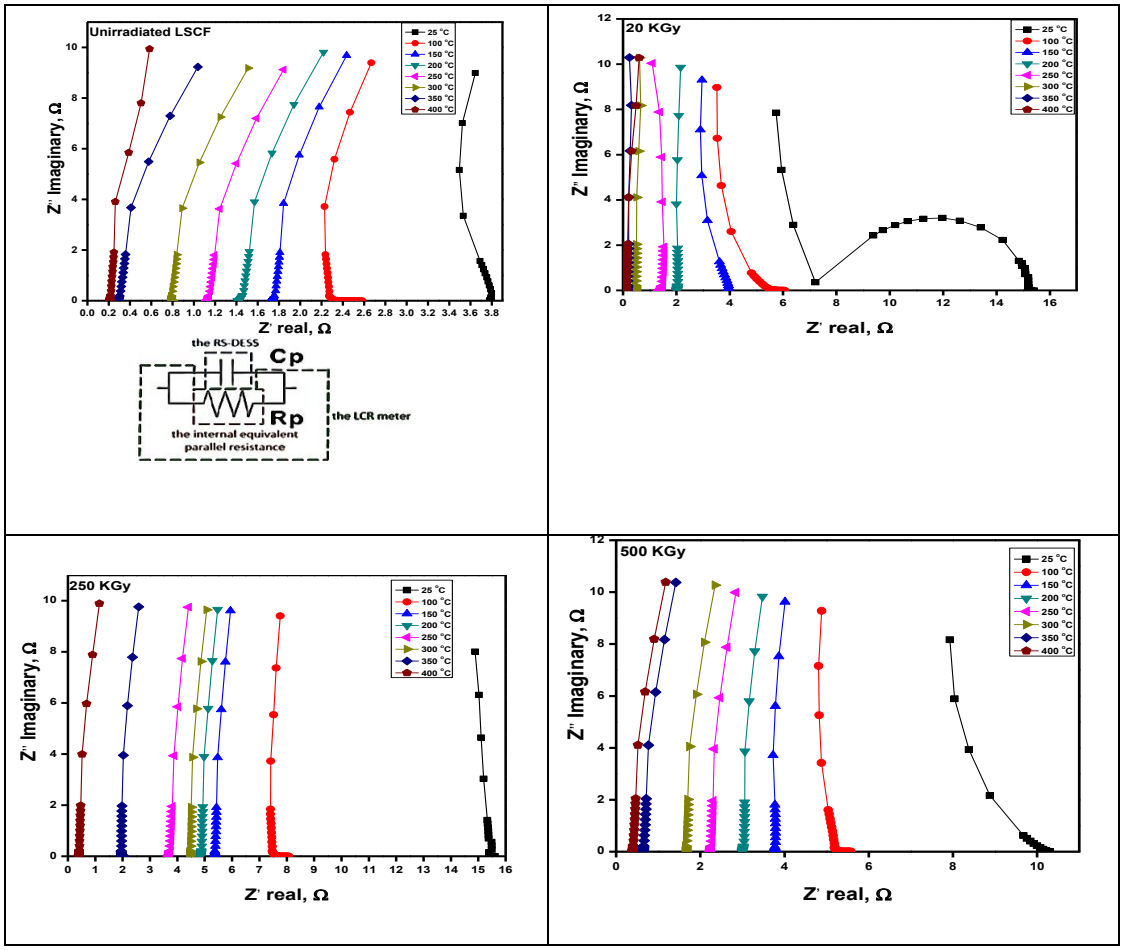

Fig. 6. Impedance spectra of unirradiated and irradiated LSCF samples measured from room temperature up to 400 oC in air using two probe techniques

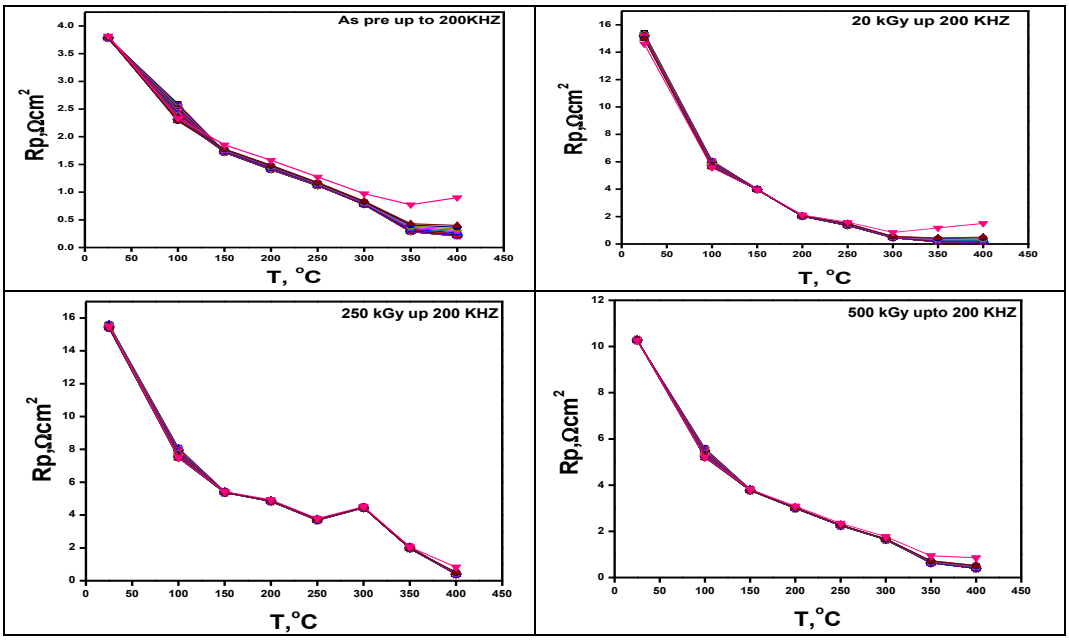

Fig. 7. Plot of Polarization resistance vs Temperature for the unirradiated and irradiated LSCF samples

TABLE 2. Area specific resistance (Ω cm^2) for the LSCF cathode samples measured at room temperature and 400°C

Sample	Unradiared LSCF	20 kGy	250 kGy	500 kGy
Rp, room temperature (Ω)	3.78	15.4	15.6	10.3
ASR, room temperature(Ω cm^2)	2.14	8.71	8.82	5.82
Rp, 400°C(Ω)	2.24E-01	1.02E-01	3.98E-01	4.05E-01
ASR, 400°C Ω cm^2)	0.1267	0.0577	0.2251	0.1396

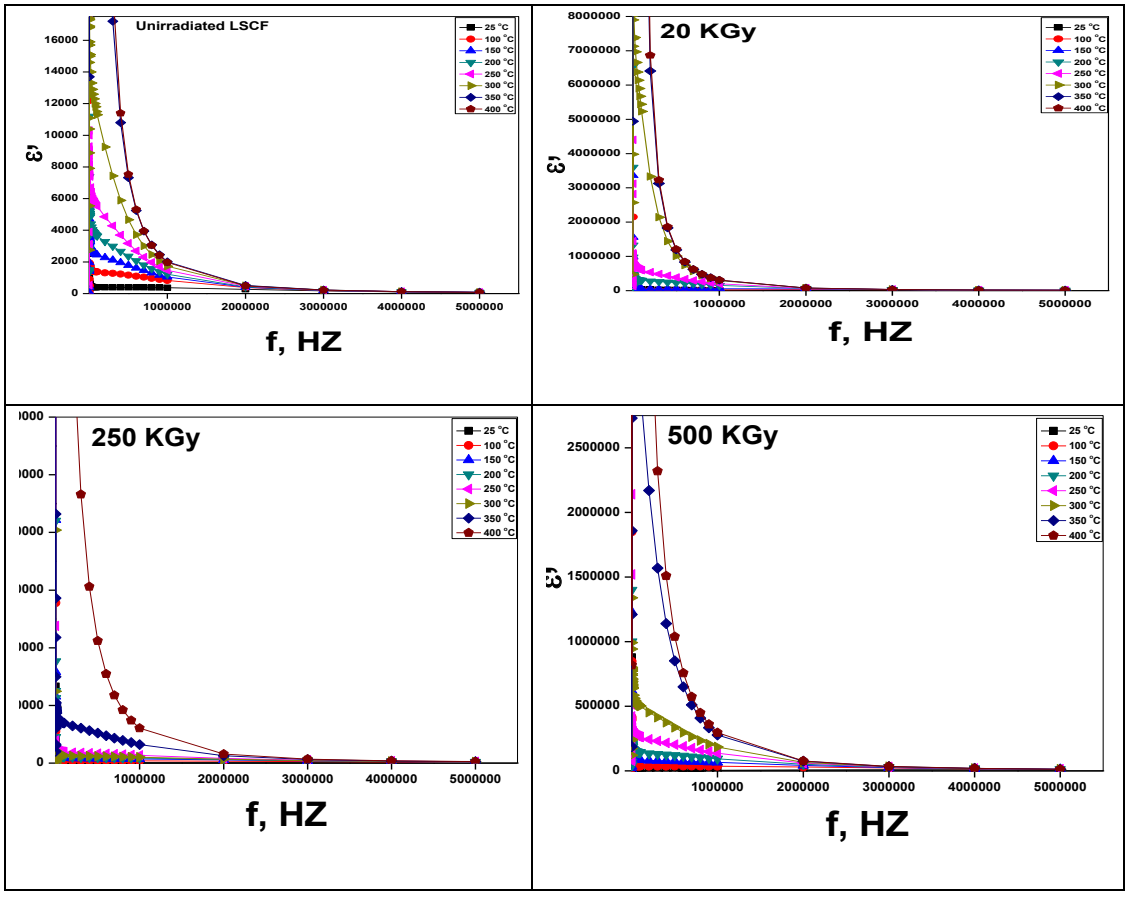

Fig. 8. Electrical ac conductivity for the unirradiated and irradiated LSCF samples

TABLE 3. Maximum ac electrical conductivity for all LSCF samples at different temperatures

Sample		Un-irradiated LSCF	20 kGy	250 kGy	500 kGy
Max.ac conductivity (S.cm^{-1})	25°C	0.0562	2.32	2.28	3.45
	100°C	0.124	8.9	6.57	9.35
	200°C	0.151	17.5	7.33	11.8
	300°C	0.274	77.9	7.95	21.6
	400°C	1.03	340	89.2	90.3

Dielectric constant

A dielectric is an electrical insulator when the dielectric is placed in an electric field, electric charges do not flow through the material as they do in a conductor, but only slightly shift from their average equilibrium positions causing dielectric polarization. From Fig. 9, it was shown that dielectric constant decreases with increasing the frequency and reaches a constant value at a high frequency for all LSCF samples (Harish et al., 2018). The effect of the frequency on the dielectric constant can be explained on

basis of interfacial polarization occurs through the hopping of electrons at grain boundary that causes for high dielectric constant at a low frequency. At a high frequency the hopping of electrons does not follow fluctuations of AC field. Consequently there is a decrease in the probability of electrons reaching grain boundary as a result the contribution of interfacial polarization falls down and that causes to a decreases in the value of the dielectric constant (Harish et al., 2018). Morever, as the temperature, crystallinalty and radiation dose increases charge carriers have enough thermal energy to move freely through the crystal causing polarization ;which results in increasing the dielectric constant of the LSCF sample.

Conclusion

Developing intermediate temperature SOFCs requires discovering new cathode materials with faster ORR kinetics. MIEC oxides such as LSCF oxides are promising alternative cathode materials to other materials such as i.e. LSM. In this paper; we carried out improvement microstructure and electrical properties such as; polarization resistance, ac conductivity and dielectric constant for LSCF cathode material using innovative approach "γ-radiation" instead of utilizing new cathode materials as they are very expensive. LSCF precursor was synthesized by sol-gel and modified sol-gel by gamma radiation technique. From the XRD results, we succeeded in obtaining pure pervoskite crystalline LSCF powders by calcining the precursor at 1100°C in air. Also, A strong impact of using new technique "radiation" on characterization physical and electrical properties for irradiated LSCF samples; where results showed that specific surface area increased from 62 to 74 m^2/g due to radiation. Furthermore,formation of oxygen vacancies increased as shown in PL spectra for the irradiated LSCF samples.

ASR, conductivity and dielectric constant were also improved due to radiation Thus, radiation technique has a great influence on selection of promising LSCF material for use as a cathode at IT-SOFCS application; where the operating performance for LSCF samples was improved.

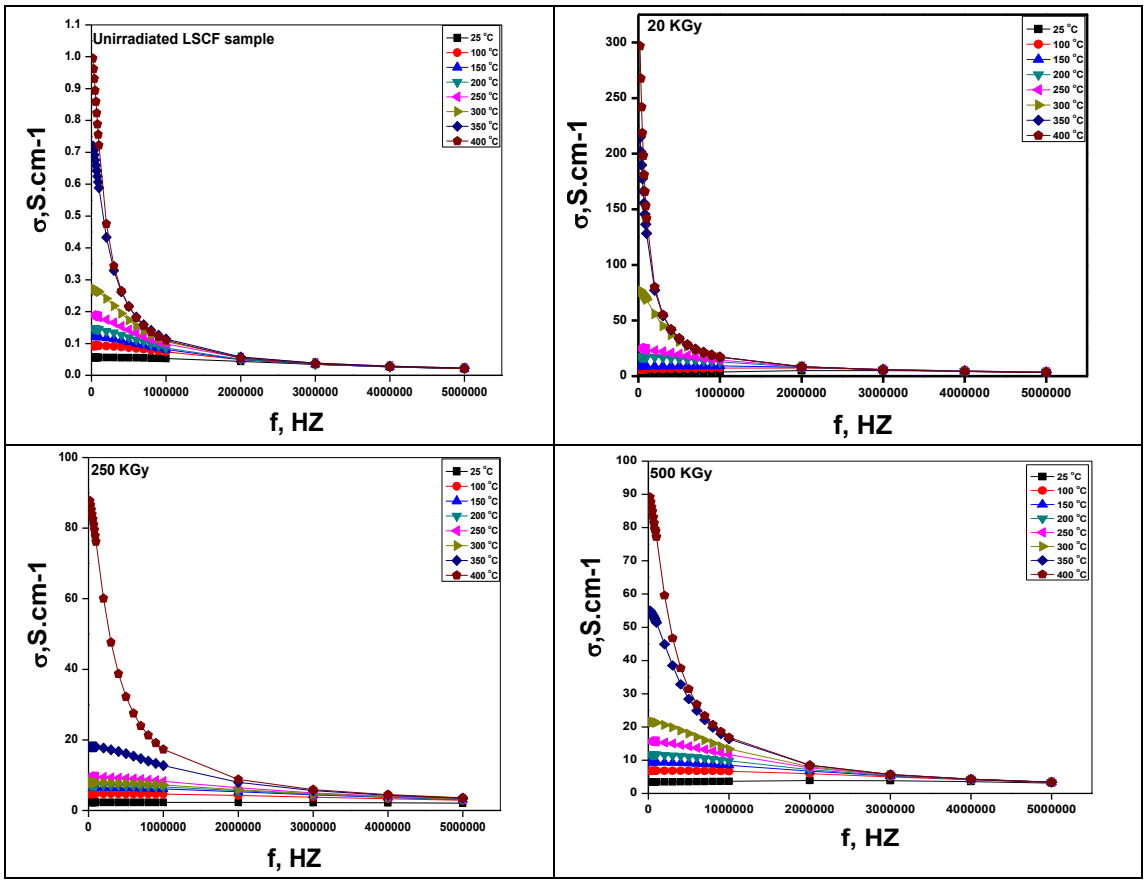

Fig. 9. Plot of dielectric constant for unirradiated and irradiated LSCF samples

References

Abd Al-Rahman, Y.M. (2013) Characterization and some applications of nano-inorganic oxides synthesized by microwave technique, *MSc Thesis.* Faculty of Science Cairo University.

Abd Malek, N.I., Ismariza I., Abdul Mutalib, J., Osman, Nafisah (2020) Characterization of LaSrCoFeO3 cathode material prepared with the aid of functionalized carbon nanotubes for proton conducting fuel cell. *AIP Conference Proceedings* 2221, 030001.

Adler, S.B. (1998) Mechanism and kinetics of oxygen reduction on porous La1−xSrxCoO3−δ electrodes. *Solid State Ionics,* **111**(1), 125-134.

Adler, S., Chen, X., Wilson, J. (2007) Mechanisms and rate laws for oxygen exchange on mixed-conducting oxide surfaces. *Journal of Catalysis,* **245**, 91-109.

Ahmed, A., Borham, E., Ibrahim, Mervat, Mahdy, A.A., Mattar, T. (2022) Enhanced performance of LSCF as a cathode material for solid oxide fuel cell. *Egyptian Journal of Chemistry,* **65**, 1-7.

Alber, K.S., Cox , J.A. (1997) Electrochemistry in solids prepared by sol-gel processes. *Mikrochim. Acta* , **127**, 131.

Ali, S.M., Abd Al-Rahman, Y.M., Galal (2012) A. catalytic activity toward oxygen evolution of LaFeO3 prepared by the microwave assisted citrate method. *Journal of Electroche mical Society*, **159**(9), 600-605.

Anand, G.T., Kennedy, L.J., Vijaya, J.J. (2013) Microwave combustion synthesis, structural, optical and magnetic properties of Zn1−xCoxAl2O4 (0≤x≤0.5) spinel nanostructures. *Journal of Alloys and Compounds*, **581**, 558-66.

Berejka, A.J. (1995) Irradiation processing in the '90's: energy savings and environmental benefits. *Radiation Physics and Chemistry*, **46**(4), 429–437.

Bi, L., Da'as, E.H., Shafi, S.P. (2017) Proton-conducting solid oxide fuel cell (SOFC) with Y-doped BaZrO3 electrolyte. *Electrochemistry Communications*, **80**, 20-23.

Cohen, R.E. (1992) Origin of ferroelectricity in perovskite oxides. *Nature*, **358**, 136-138.

Deshmukh, S.B., Bari, R.H. (2015) Nanostructured ZrO_2 thin tilms reposited by epray pyrolysis techniques for ammonia gas sensing application *International Letters of Chemistry Physics and Astronomy,* **56**, 120-130.

El-Mallah, H.M. (2012) AC electrical conductivity and dielectric properties of perovskite (Pb, Ca) TiO_3 ceramic. *Acta Physica Polonica*, **122**,1-6.

Ghouse, M., Al-Yousef, Y., Al-Musa, A., Al-Otaibi, M.F. (2010) Preparation of La0.6Sr0.4Co0.2Fe 0.8O3 nanoceramic cathode powders for solid oxide fuel cell (SOFC) application. *International Journal of Hydrogen Energy,* **35**, 9411–9419.

Gu, H., Chen, H., Gao, L., Guo, L. (2009) Electrochemical properties of LaBaCo2O5þd-Sm0.2Ce0.8O1.9 composite cathodes for intermediate-temperature solid oxide fuel cells. *Electrochimica Acta*, **54**(70), 94-8.

Harish, B.M., Yallappa, S., Avinash, B.S., Chaturmukha, V.S., Jayanna, H.S. (2018) Temperature dependent dielectric constant and AC conductivity of porous CeO_2 nanoparticles obtained by solution combustion method. *Journal of Nanofluide*, **7**, 1-7.

Hsu, C-S, Hwang, B-H (2006) Microstructure and properties of the La0.6Sr0.4Co0.2Fe0.8O3 cathodes prepared by electro static assisted ultrasonic spray pyrolysis method. *Journal of The Electrochemical Society*, **153**, A1478.

Hussain, A.M., Pan, K-J, Robinson, I.A., et al (2016) Stannate-basedceramic oxide as anode materials for oxide-ion conducting lowtemperature solid oxide fuel cells. *Journal of The Electrochemical Society*, **163**, F1198.

Hwang, H.J., Ji-Woong, M.B., Seunghun, L.A., Lee, E.A. (2005) Electrochemica performance of LSCF-based composite cathodes for intermediate temperature SOFCs. *Journal of Power Sources,* **145**(2), 243-8.

Ismariza, I., Osman, Nafisah, Abdul Mutalib, J. (2020) La0.6Sr0.4Co0.2Fe0.8O3−δ powder: a simple microstructure modification strategy for enhanced cathode electrochemical performance. *Journal of Sol-gel and Technology,* **2221**(1), 1-6.

Jin, S., Tiefel, T.H., Mccormack, M., Fastnacht, R.A., Ramesh, R., Chen, L.H. (1994) Thousandfold

change in resistivity in magnetoresistive la-ca-mn-o films. *Science*, **264**, 413-415.

Kaur, J., Anand, K., Kaur, A., Singh, R.C. (2018) Sensitive and selective acetone sensor based on Gd doped WO3/reduced graphene oxide nanocomposite. *Sensors and Actuators B: Chemical,* **258**, 1022–1035.

Kernazhitsky, L., Shymanovska, V., Naumov, V., Fedorenko, L., Kshnyakin, V., Shcherban, N., Filonenko, S., Baran, J. (2017) Room temperature photoluminescence of mixed titanium-manganese oxides. *Journal of Luminescence,* **187**, 521–527.

Kostogloudis, G.Ch., Ftikos, Ch. (1999) Properties of A-site-deficient $La_{0.6}Sr_{0.4}Co_{0.2}Fe_{0.8}O_{3-\delta}$-based perovskite oxides. *Solid State Ionics*, **126**(1) ,143-151.

Laruelle, S., Grugeon, S., Dupont, L., Tarascon, J.M, (2000) Nano-sizedtransition-metal oxides as negative-electrode materials for lithium-ionbatteries. *Nature*, **407**, 496–499.

Leng, Y., Chan, S.H., Liu, Q. (2008) Development of LSCF-GDC composite cathodes for low-temperature solid oxide fuel cells with thin film GDC electrolyte. *International Journal of Hydrogen Energy,* **33**, 3808–3817.

Lev, O., Wu, Z. (1997) Sol−Gel Materials in Electrochemistry. *Chemistry of Materials,* **9**, 2354.

Luyten, J., Buekenhoudt, A., Adriansens, W., et al. (2000) Preparation ofLaSrCoFeO3-x membranes. *Solid State Ionics*, **135**, 637–642.

Liu, M., Wang, D. (1995) Preparation of $La_{1-z}Sr_zCo_{1-y}Fe_yO_{3-x}$ thin films, membranes, and coatings on dense and porous substrates. *Journal of Materials Research,* **10**, 3210.

Mahmud, L.S., Muchtar, A., Somalu, M.R. (2017) Challenges in fabricating planar solid oxide fuel cells: a review. *Renewable and Sustainable Energy Reviews,* **72**, 105–116.

Marinha, D., Hayd, J., Dessemond, L., et al. (2011) Performance of (La, Sr)(Co,Fe)O3-x double-layer cathode films for intermediate temperature solid oxide fuel cell. *Journal of Power Sources,* **196**, 5084–5090.

Mefford, J.T., Hardin, W.G., Dai, S., Johnston, K.P., Stevenson, K.J. (2014) Anion charge storage through oxygen intercalation in LaMnO3 perovskite pseudocapacitor electrodes, *Nature Materials,* **13**, 726.

Murray, E.P., Sever, M.J., Barnett, S.A. (2002) Electrochemical performance of (La, Sr)(Co, Fe) O3e (Ce, Gd)O3 composite cathodes. *Solid State Ionics,* **148**(1e2), 27-34.

Ng, J., Xu, S., Zhang, X., Yang, H.Y., Sun, D.D. (2010) Hybridized nanowires and cubes: a novel architecture of a heterojunctioned TiO2/SrTiO3 thin film for efficient water splitting. *Advanced Functional Materials,* **20**(24), 4287-94.

Nie, L., Liu, Z., Liu, M., et al (2010) (LSCF) cathodes with graded microstructure fabricated by tape casting. *Journal of Electrochemical Science and Technology*, **1**, 50–56.

Perry Murray, E., Sever, M., Barnett, S. (2002) Electrochemical performance of (La, Sr)(Co, Fe) O3e(Ce, Gd)O3 composite cathodes. *Solid State Ionics*, **148**, 27-34.

Qianqian, Ji., Lei, Bi., Jintao Zhang, Haijie Cao, Zhao, X.S. (2020) The role of oxygen vacancies of ABO3 perovskite oxides in the oxygen reduction reaction. *Energy & Enivromental Science*, **13**, 1-63.

Raj Mani, Ravindra Kumar Gautam, Sushmita Banerjee, Anoop K. Srivastava, Amita Jaiswal, Chattopadhyaya, M.C. (2015) *Asian Journal of Research in Chemistry,* **8**(6), 390.

Richardson, R.A., Cotton, J.W., Mark Ormerod, R. (2004) Influence of synthesis route on the properties of doped lanthanum cobaltite and its performance as an electrochemical reactor for the partial oxidation of natural gas. *Dalton Transactions*, **19**, 3110–3115.

Sreeram, K.J., Aby, C.P., Nair, B.U., Ramasami, T. (2008) Colored cool colorants based on rare earth metal ions. *Solar Energy Materials and Solar Cells,* **92**(11), 1462-7.

Suzuki, T., Jasinski, P., Anderson, H.U., Dogan, F. (2004) Role of composite cathodes in single chamber SOFC. *Journal of The Electrochemical Society*, **151**(10), A1678-82.

Tai, L.-W., Nasrallah, M.M., Anderson, H.U., Sparlin,

D.M., Sehlin, S.R. (1995) Structure and electrical properties of La1- xSrxCo1-yFeyO3. Part 2. The system La1- xSrxCo0.2Fe0.8O3. *Solid State Ionics,* **76**, 273-283.

Tandon, S., Gupta (1970) Measurement of forbidden energy gap of semiconductors by diffuse reflectance technique. *Physica Status Solidi (B*), **38**(1), 363-7.

Wang, S., Katsuki, M., Dokiya, M., Hashimoto, T. (2003) High temperature properties of $La_{0.6}Sr_{0.4}Co_{0.8}Fe_{0.2}O_{3-\delta}$ phase structure and electrical conductivity. *Solid State Ionics,* **159**(1-2), 71.

Wang, W., Xu, M., Xu, X., Zhou, W., Shao, Z. (2019) Reducing detrimental defects for high-performance metal halide perovskite solar cells. *Angewandte Chemie International Edition*, **58**, 2-19.

Wanqin Jin, Shiguang Li, Pei, Huang, Nanping Xu, Jun Shi, (2000) Fabrication of $La_{0.2}Sr_{0.8}Co_{0.8}Fe_{0.2}O_{3-\delta}$ Mesoporous membranes on porous supports from polymeric precursors. *Journal of Membrane Science,* **170**, 9.

Yin, J.-W., Y.-M. Yin, J. Lu, C. Zhang, N.Q. Minh, Z.-F. Ma, (2014) Structure and properties of novel cobalt-free oxides NdxSr1–xFe0.8Cu0.2O3−δ ($0.3 \leq x \leq 0.7$) as cathodes of intermediate temperature solid oxide fuel cells. *Journal of Physical Chemistry C,* **118**, 13357–13368.

Zhou, W., Ge, L., Ran, R., et al (2008) Facile autocombustion synthesis of La0.6Sr0.4Co0.2Fe0.8O3- δ (LSCF) perovskite via a modified complexing sol-gel process with NH4NO3 as combustion aid. *Journal of Alloys and Compounds*, **450**, 338–347.

Zhu, Y.L., Zhou, W., Yu, J., Chen, Y.B., Liu, M.L., Shao, Z.P. (2016) Enhancing electrocatalytic activity of perovskite oxides by tuning cation deficiency for oxygen reduction and evolution reactions. *Chemistry of Materials*, **28**, 1691-1697.